Received: 4 June 2020 | Revised: 28 August 2020 | Accepted: 20 October 2020

DOI: 10.1111/jace.17556

Check for updates

Journal of the American Ceramic Society

ORIGINAL ARTICLE

Erosion behavior of Y_2O_3 in fluorine-based etching plasmas: Orientation dependency and reaction layer formation

Moritz Kindelmann[1,2] | **Mark Stamminger**[3] | **Nino Schön**[1,4] | **Marcin Rasinski**[1] | **Rüdiger-A. Eichel**[1,4,5] | **Florian Hausen**[1,4,5] | **Martin Bram**[1] | **Olivier Guillon**[1,2,5]

[1]Institute of Energy and Climate Research, Forschungszentrum Jülich GmbH, Jülich, Germany

[2]Institute of Mineral Resources Engineering, RWTH Aachen University, Aachen, Germany

[3]Institute of Experimental Physics II, Ruhr-Universität Bochum, Bochum, Germany

[4]Institute of Physical Chemistry, RWTH Aachen University, Aachen, Germany

[5]JARA-Energy, Jülich Aachen Research Alliance, Jülich, Germany

Correspondence
Moritz Kindelmann, Forschungszentrum Jülich GmbH, Institute of Energy and Climate Research, 52425 Jülich, Germany.
Email: m.kindelmann@fz-juelich.de

Funding information
ProjektDEAL

Associate Editor: Professor Theodore Besmann

Abstract

Even though advanced ceramics are widely applied as consumables in semiconductor etching processes, the erosion mechanisms and connected surface phenomena are not fully understood. Through the interaction with reactive species and ion bombardment during the plasma exposure, oxide ceramic materials like Y_2O_3 are eroded by a physicochemical mechanism. In this study, fundamental phenomena of surface-plasma interactions were investigated directly at the surface as well as in the near-surface region after exposure to fluorine-based etching plasmas. A straightforward re-localization technique was used to investigate the microstructural features before and after the plasma exposure for up to 2 hours. Electron microscopy methods (scanning electron microscopy, electron backscatter diffraction) were coupled with atomic force microscopy, secondary ion mass spectroscopy, and transmission electron microscopy to study the surface topography and the corresponding reaction layer. Direct correlation of the microstructure before plasma exposure with the surface topography reveals a novel orientation-dependent erosion mechanism that forms plateau-like structures. Furthermore, the in-depth analysis of the near-surface area highlights the influence of the applied bias voltage on the physical damage and chemical gradient formation due to plasma exposure. The combined investigation of surface morphology and near-surface properties reveals new fundamental aspects of the erosion behavior of polycrystalline yttria in CF_4-based etching plasmas.

KEYWORDS

chemical durability, etchants/etching, yttrium/yttrium compounds

1 | INTRODUCTION

The rapid development and increasing complexity of integrated electronic devices require challenging manufacturing processes, which are used to produce state-of-the-art electronic devices. In addition to stereolithography, etching techniques are essential during all processing steps. Long-term etching treatments, high bias voltages, and aggressive plasma

This is an open access article under the terms of the Creative Commons Attribution-NonCommercial License, which permits use, distribution and reproduction in any medium, provided the original work is properly cited and is not used for commercial purposes.
© 2020 The Authors. Journal of the American Ceramic Society published by Wiley Periodicals LLC on behalf of American

chemistries tighten the exposure profile of plasma-facing components inside the manufacturing device.[1]

Advanced ceramic materials like yttria (Y_2O_3) are increasingly applied inside etching chambers due to their high stability in contact with halogen-based etching chemistries.[2-4] Due to the formation of nonvolatile reaction products on the component surface, erosion rates of ceramic materials are lower by orders of magnitude compared to the erosion of high-quality quartz glass components, which decompose through the formation of gaseous reaction products.[5] However, the formation of solid reaction products increases the risk of particle formation, which can be fatal during the processing of sensitive semiconductor components.[6]

Various options exist to deposit yttria as a functional component inside plasma etching devices. Foremost among them is the development of functional coatings on quartz or alumina substrates, which has been proposed to increase the stability of the substrate during operation against rapid erosion. Different coating techniques are used to apply yttria: Iwasawa et al. introduced aerosol deposition (AD) as a novel coating technology for yttria on quartz substrates.[3] Jung et al. and Ashizawa et al. applied AD to other rare earth compounds and investigated their erosion behavior.[7,8] Furthermore, thermal spray techniques like atmospheric plasma spray[9,10] and suspension plasma spray[11,12] were used for yttria coatings aiming to increase the durability of etching equipment.

Besides functional coatings, the preparation and application of bulk yttria were investigated. Up to now, they tended to be processed by pressureless sintering[13] or by a combination of sintering with subsequent hot isostatic pressing.[14] Further investigations into bulk compounds focus on material functionalization by adding conductive phases,[15] alumina-yttria composites,[16] or the use of fluorine-containing yttrium materials.[17-19]

The first studies focusing on the understanding of erosion mechanisms of yttria used X-ray photoelectron spectroscopy (XPS). In these works, the fluorination (in CF_4- and SF_6-based plasmas) and chlorination (in Cl_2-based plasmas) of the surface was determined, highlighting the role of chemical surface interactions as an important factor in the erosion process.[20,21] Initially, Miwa et al. described the fluorination process as a reaction between deposited fluorocarbons, which break the Y–O bonds and enable a reaction of the Y atoms at the surface with F, forming an upper layer of YF_X,[21] which is prone to be removed by Ar^+ sputtering.[23] Further insight into the erosion process was given by Kim et al. who showed the formation of a fluorine gradient from the surface to the bulk.[4] Furthermore, a significant difference between sputtering rates of aluminum oxide and yttria and their corresponding fluorides was found.[23] The erosion process of yttria was attributed to physicochemical mechanisms, which are dependent on fluorination of the surface and on the related physical sputtering properties, both of which determine the overall resistance against erosion.

Especially when focusing on the active mechanisms during etching, microstructural defects like roughness and porosity play a predominant role in erosion leading to a crater-like surface topography.[14,24] Most polycrystalline materials show such microstructural defects, which are especially likely to appear if the processing of the material is based on powder technologies. Therefore, this study will focus on preparing nearly defect-free materials and investigate the influences of microstructure and applied bias voltage on the chemical interactions and physical erosion of polycrystalline yttria. Specific focus will be given to the influence of the microstructural properties at the surface (crystalline orientation, grain boundaries). Orientation-dependent erosion during plasma exposure has been described for metals (stainless steel, tungsten) subjected to fusion plasmas.[25-27] Comparable observations have not been described for ceramics, which is why further research into the mode of erosion (homogeneous or selective) is needed. To exclude interfering surface defects, field-assisted sintering technique/spark plasma sintering (FAST/SPS) is used to achieve fully densified, highly pure yttria samples.[28]

2 | EXPERIMENTAL PROCEDURE

High-purity Y_2O_3 powder (99.99 % purity; KDL Resources) was used as the starting material. The content of elemental impurities was investigated by using inductively coupled plasma (ICP-MS; Agilent 7900). The powder contained traces of 4 ppm Si, 20.0 ppm Ca, 1.9 ppm Zn, 0.2 ppm Sr, 0.6 ppm Ba, and 0.1 ppm Ce. The content of critical elements with respect to an application in plasma-etching devices like Co, Na, Ni, and Ti was below the detection limit. The primary crystallite size of the yttria powder was approximately 60 ± 17 nm (measured by TEM). The powder was heavily agglomerated with an average agglomerate size of 5.2 ± 0.1 μm (measured by laser granulometry; LA-950 HORIBA Scientific), making it impossible to process it to full density by conventional pressing and sintering.

Therefore, FAST/SPS was used to produce highly dense polycrystalline yttria samples. Samples were prepared in a FAST/SPS system (HP-D5; FCT Systeme) using a graphite tool with a diameter of Ø12 mm. All FAST/SPS cycles were done at 1500°C using a uniaxial pressure of 50 MPa, a heating rate of 100 K/min, and a dwell time of 10 minutes. After ejection of the samples, graphite residues were removed, and all samples were thermally treated in air in a chamber furnace at 1200°C for 4 hours to regain oxygen stoichiometry. Afterwards the sample thickness was reduced to around 1 mm by grinding and the plasma-facing surface was mirror polished with 1 μm diamond paste

to minimize the influence of surface roughness during the plasma treatment. Before being exposed to the reactive plasma atmosphere, markers were placed on the sample surface using a commercial Vickers hardness testing machine (Duramin A-300; Struers) following the procedure shown in Figure S1. Cracks starting from the corners of the Vickers indentation were used to locate the same area of interest before and after the plasma treatment. With this strategy, it became possible to investigate microstructural changes that directly depend on the exposure conditions, enabling sound conclusions to be drawn regarding the related erosion mechanisms and a reliable distinction to be made between homogeneous (mode I) or selective (mode II) erosion modes.

The characterization of the sample surface in the as-polished state focused on the microstructural features and the crystalline orientation. To this end, scanning electron microscopy (SEM; Zeiss Cross Beam XB540) and electron backscatter diffraction (EBSD; Oxford instruments) were used. Special precautions (carbon coating, thermal treatment in air at 800°C for 5 hours) were taken to remove all conductive coatings and facilitate a contamination-free surface to exclude any external influences on the plasma-surface interactions.

Subsequently, etching experiments were conducted in an experimental ICP reactor using Ar (5.0 sccm), CF_4 (1.0 sccm), and O_2 (0.3 sccm) as a fixed gas composition. The working pressure during the plasma exposure was set to 0.02 mbar. The IC power was kept constant for all experiments at 600 W and the bias voltage was varied among 50, 150, and 300 V. All samples were exposed for 120 minutes to ensure comparability between experiments with varying bias voltages.

After removal from the plasma chamber, the surface topography of the samples was studied by atomic force microscopy (AFM; Bruker Dimension Icon). The topography data generated by AFM in tapping mode were visualized using the software package Gwyddion. The cantilevers used to perform the measurements were ppp-NCHR from Nanosensors (NanoWorld AG). Postprocessing of the topographic data was performed using the align rows as well as the remove background function. For an advanced analysis of the relationship between surface topography and grain orientation, the Euler angles Φ and φ_2 were correlated with topographic AFM data. The height difference Δh (taken from the median height of the grain) between the plateaus formed after plasma exposure was measured. The plateau with the highest erosion rate was used as the zero reference. For statistical reasons, at least 160 grains were considered and Δh was correlated with the crystalline orientation of the respective grain before plasma exposure (Figure S2).

For characterization of the reaction layer formed on the sample surface during plasma exposure, transmission electron microscopy (TEM; Tecnai F20; FEI) was done in scanning TEM and high resolution TEM mode. Therefore, focused ion beam lamellae were cut at specific areas of interest.

Additionally, TEM results were accompanied by time of flight secondary ion mass spectroscopy (TOF-SIMS; ION-TOF). Concentration profiles of F-, O-, and Y- ions were measured up to a depth of 100 nm for characterization of chemical gradients formed during plasma exposure. Therefore, Cs ions (1 keV, 57 nA) were used to remove material forming a 300×300 µm sputter crater and Bi ions (30 keV, 26 pA) were used for elemental analysis in the center of the measurement area. Yttria samples consolidated by FAST/SPS and exposed to fluorine plasmas using DC self-bias voltages of 50, 150, and 300 V were measured up to depths of 100 nm from the sample surface.

3 | RESULTS AND DISCUSSION

3.1 | Topographic phenomena and orientation dependency

At first, the change of the surface topography of polished Y_2O_3 samples before and after plasma treatment (2 hours, 150 V) was investigated. Figure 1a,c show SEM images of the polished sample surface before the exposure. When polished, almost no topographical features are visible. This enables the crystalline orientation to be depicted in secondary electron (SE-SEM) images after optimization of the imaging parameters. Furthermore, the level of intergranular porosity is low. Therefore, the samples are suitable for detailed investigation of the interaction between bulk polycrystalline Y_2O_3 and reactive plasma. Superposition of significantly increased erosion at pores and surface roughness can be excluded to a large extent.[24]

Figure 1b, d shows the same area after reactive plasma treatment for 2 hours. At higher magnification, different surface morphologies can be observed (Figure 1d), which hints at differences regarding the ion sputtering and the fluoride layer formation depending on the grain orientation. These conditions lead to a rough surface topography exhibiting small, nanometer-sized pores within the grains after the plasma exposure (for more details see Figure S3). Larger pores—residuals from incomplete densification during sintering—became rounded after plasma treatment due to erosion predominantly affecting sharp corners. This observation is consistent with the literature,[14,24] but will not be considered further in this study.

Additionally, both micrographs show the formation of a plateau-like surface topography. Due to the visible orientation contrast of the grains, it became clear that the plateaus are directly related to the primary grain structure. Certain grain orientations exhibit a slightly increased tendency to become eroded, while others tend to have a better resistance

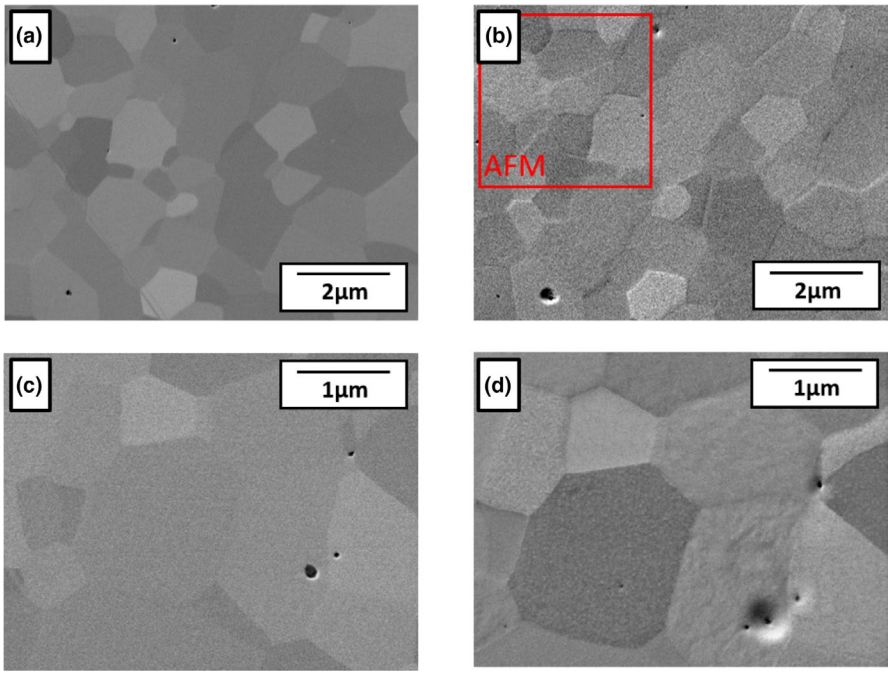

FIGURE 1 SE-SEM images of the microstructure at the surface before (a, c) and after plasma exposure for 2 h with a bias voltage of 150 V (b, d) [Color figure can be viewed at wileyonlinelibrary.com]

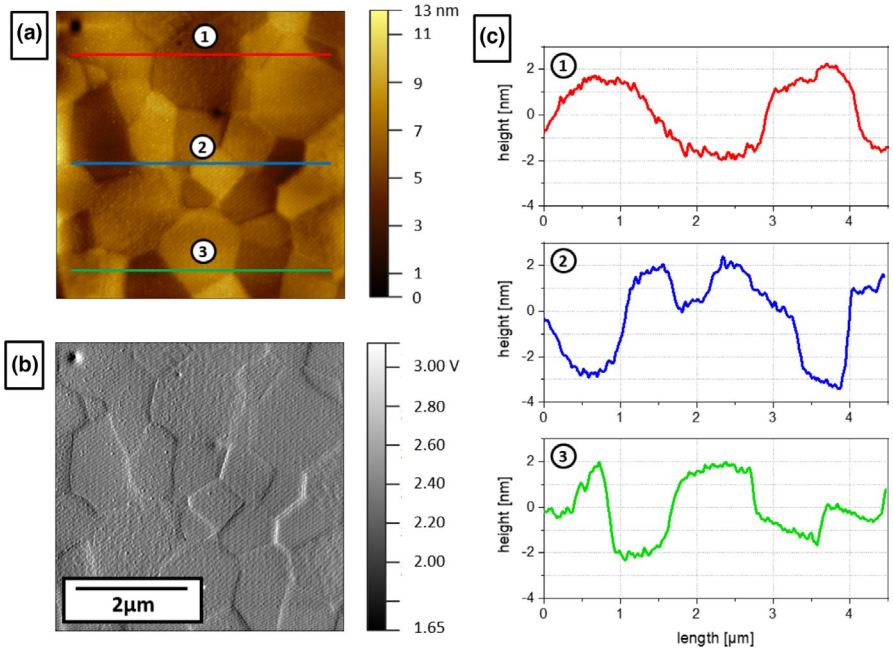

FIGURE 2 Atomic force microscopy scan of the surface after plasma exposure for 2 h at a bias voltage of 150 V (highlighted area in the scanning electron microscopy image from Figure 1; tilted by 90°), showing the surface as a topography image (a) and as amplitude error (b). c, Line scans at three positions extracted from the topography image (a) [Color figure can be viewed at wileyonlinelibrary.com]

against the plasma attack. Similar observations have been reported by Balden et al for stainless steel[25] and Voitsenya et al. and Rasinski et al. for tungsten materials,[26,27] which are used in components of fusion reactors. In these studies, the experimental set-up was comparable to a certain extent. The main differences were the ion flux and the reactive species (H^+, Ar^+, D^+-Ar^+) characteristic for the plasma in a fusion reactor. The authors found that surface erosion depended heavily on grain orientation. It is expected that such an erosion mechanism will occur in yttria as well, but not as clearly pronounced as in metals.

To gain a better understanding, the topography of the eroded surface was investigated by AFM (Figure 2). The area considered for this study is marked by a red square in Figure 1b. The grain structure—represented through different grayscales in the SEM image—is likewise visible in the AFM topography mapping. AFM measurements confirm that the height levels of the distinct plateaus are directly connected to the primary grain structure. Thus, a direct connection between the grain orientation and the resistance against erosion by reactive plasmas also seems reasonable for ceramics such as Y_2O_3. Compared to metals used as plasma-facing materials in fusion reactors,

the height relief formed after plasma exposure is comparably minor, which can be correlated with the low sputtering yields observed for ceramic materials in comparison to metals.[23,29] For a better visualization of height deviations in surface topography, line profiles derived from the AFM scan in Figure 2a) are shown in Figure 2c). The exposure resulted in clearly pronounced steps between the different plateaus. Although some of the plateaus do not show an even surface, a significant height difference between all grains is apparent.

Due to the low average etch depth of 47 ± 5 nm (measured by profilometry) after an exposure to 150 V for 180 minutes (plasma composition as presented in Section 2), the orientation dependent difference in etch depth can have a measurable influence on the erosion of yttria.

In addition to the erosion depending on the grain orientation, the grains reveal a different surface morphology, as indicated by the unevenness in the amplitude image (Figure 2b) on certain grains. This could be caused by the active dual erosion mechanism, which on the one hand depends on the formation of the fluorine reaction layer, but on the other hand relies heavily on the physical sputtering of these layers.

A deeper understanding of the relationship between grain orientation and the surface topography after plasma exposure is enabled by applying the relocalization method, which is based on a combination of EBSD and AFM (Figure 3). Again, a selected area before (Figure 3a) and after (Figure 3b) the plasma exposure is shown. As already discussed, the plasma treatment leads to the formation of a surface topography correlated with the polycrystalline microstructure of yttria. The comparison of crystalline orientation (represented through inverse pole figure (IPF) color) and the height topography of selected characteristic grains (highlighted through red arrows) reveal that crystallites that have a comparable IPF color do not necessarily have the same height level and vice versa. As individual comparison of selected grains does not reveal a direct correlation between orientation and erosion depth, a comprehensive analysis of all EBSD and AFM data displayed in Figure 4 was conducted following the procedure explained in the experimental part.

The detailed analysis of all grains is plotted in two graphs (Figure 4), which show the height difference Δh of 160 grains plotted against their Euler angles Φ and φ_2. Figure 4a shows the average height difference Δh of all samples using maximum and minimum values as error bars. To better distinguish the different height levels, a color key is used. Although the dataset is subjected to a considerable amount of scatter, angles in the range 0°-10° and 40°-45° tend to show the largest height difference. In turn, at intermediate angles plasma erosion tends to be less pronounced. The lowest values of Δh are observed at angles of 15°-30°. As grains with an average topographic height in the range 5-10 nm do not have a predominant orientation, we focus on the minima and maxima of the topographic relief to discuss the influencing factors behind the erosion mechanism. Therefore, further details of the relationship between topography and grain orientation are given in Figure 4b. In this figure, the rotation angle φ_2 is also shown, which ranges from 0° to 180°. The color key for the Δh value is maintained. Areas representing the maximum values of Δh are marked by a red rectangle, while areas representing the minimum values are marked by a blue rectangle. It becomes obvious that the maximum values of Δh (marked red) show a broad distribution over all displayed angles, while the minimum values of Δh (marked blue) tend to accumulate between $\Phi = 15°\text{-}30°$ and $\varphi_2 = 40°\text{-}120°$. Due to the lack of data values for certain orientations, it is only possible to show a general trend so far.

The rotation of a cubic crystal from the angle $\Phi = 0°$ to $\Phi = 45°$ can be associated with the plane tilting from the (001) plane to the (011) plane (with respect to the normal direction), which leads to a change in the alignment of atomic rows inside the lattice structure depending on the angle Φ. A similar effect has been reported by Roosendahl et al for

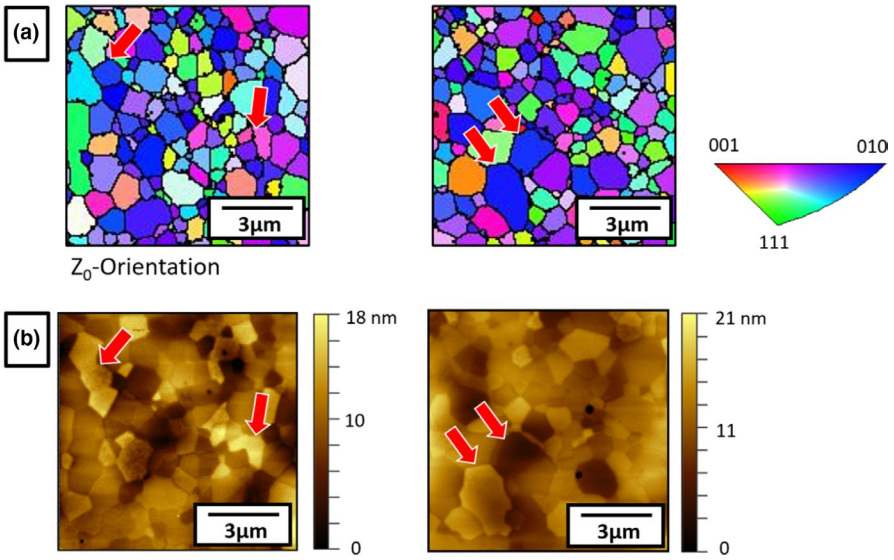

FIGURE 3 a, Electron backscatter diffraction orientation mapping at the surface before the plasma exposure in the Z_0 direction. b, Corresponding atomic force microscopy topography at the same position after the plasma exposure for 2 h at a bias voltage of 150 V (arrows highlight grains with comparable IPF colors and different heights and vice versa) [Color figure can be viewed at wileyonlinelibrary.com]

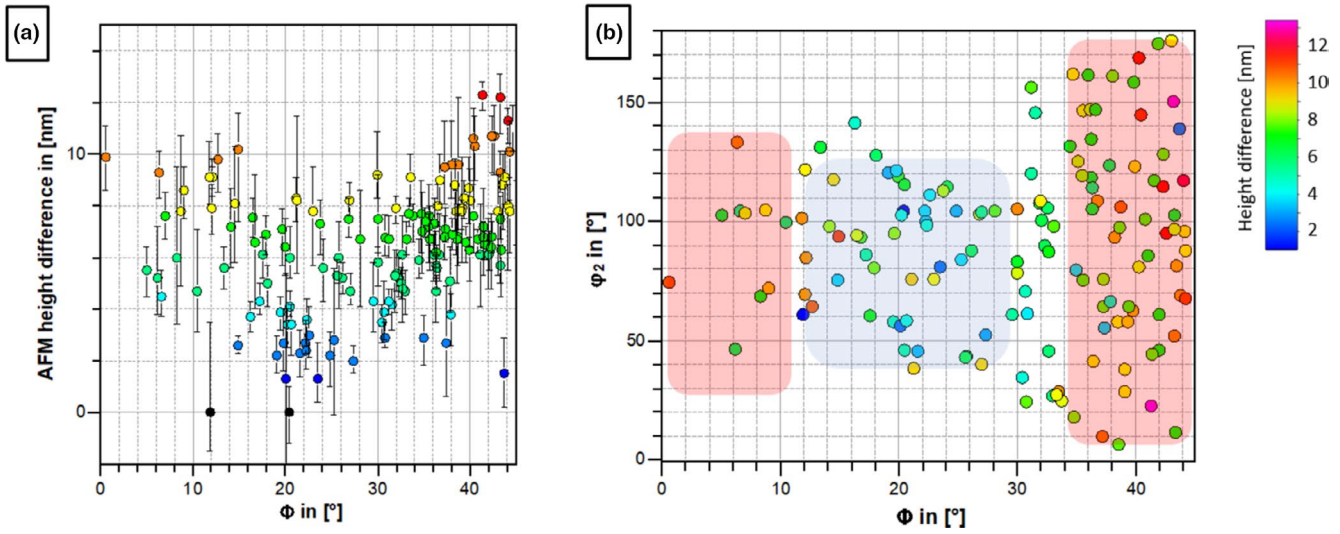

FIGURE 4 a, Topographic height difference Δh displayed depending on the Euler angle Φ and (b) depending on Φ and φ_2 representing the rotation of the crystal in 3D. The height difference Δh is the median value derived from atomic force microscopy measurements using maximum and minimum values as deviation bars [Color figure can be viewed at wileyonlinelibrary.com]

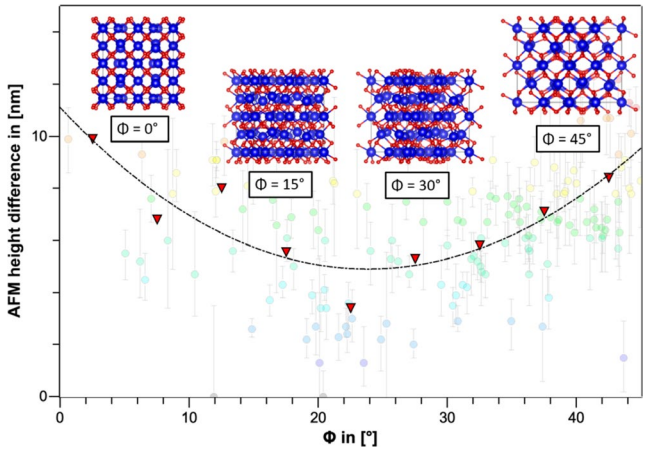

FIGURE 5 Distribution curve fitted to median height values of the data set representing the height difference Δh as a function the rotation angle Φ (measured data in the background). Each median value summarizes all data points in a range of 5°. Additionally, crystal structures at certain rotation angles ($\Phi = 0°$, 15°, 30°, 45°) are displayed [Color figure can be viewed at wileyonlinelibrary.com]

metals.[29] They found a dependence of the tilt of the plane on the sputtering yield for various metal single crystals. In the study, Cu, Ni, and semiconducting materials such as Ge and InSb were considered, which showed distinct minima for incidence angles highly aligned with certain crystal planes. The effect of crystalline orientation-dependent erosion rates in metal single crystals has been described by Onderlinden using a channeling model.[30] In this model, it is assumed that accelerated ions from the plasma that are aligned with a certain crystal direction (named "transparent" direction by the author) can be channeled along the crystal plane and therefore do not contribute to the sputtering of the material. The unaligned part of the incident ion beam contributes to the sputtering of the crystal by physically interacting with the surface atoms. This effect leads to the preferential removal of surface material. A similar effect is also utilized for crystalline alignment in ion beam-assisted deposition (IBAD). Here, a deposited layer is particularly sputtered during processing, which leads to a pronounced texture of the film.[31] Molecular dynamic simulations were conducted by Dong et al. with the aim of understanding the mechanisms responsible for the IBAD of Al[32] and MgO.[33] In this study, the relationship between crystal orientation and sputtering yield was explained based on channeling theory. The appropriateness of IBAD for the deposition of textured films clearly demonstrates the correlation between the sputtering rate and the crystal orientation. In this study, a related effect has been found for a polycrystalline material.

Adapting the concept of ion channeling and preferential sputtering to the phenomena observed in plasma-exposed Y_2O_3 helps to explain the underlying mechanisms. Therefore, Figure 5 displays a distribution curve of the height difference Δh as a function of the angle Φ (measured data is displayed in the background). Additionally, crystal structures at certain rotation angles ($\Phi = 0°$, 15°, 30°, 45°) are included in the graph as well to show crystal planes which exhibit an orientation able to allow Ar^+ ion channeling along the respective directions. In the case of yttria, a higher probability of ion channeling is expected for the rotation angles $\Phi = 0°$ and $\Phi = 45°$, which are equivalent to the (001) and (011) plane, respectively. Analysis of the topographic data exhibits that the lowest sputtering yields could be measured near highly "transparent" crystallographic planes and the highest yields were predominantly measured in a range between $\Phi = 15°$ and $\Phi = 30°$. Although other influencing factors such as

unfocused ion bombardment and the presence of a highly reactive species have to be taken into account, our results reveal predominantly orientation-dependent sputtering of polycrystalline yttria.

The described orientation-dependent erosion mechanism is highly dependent on the exposure of the Y_2O_3 surface to high ion energies. This could limit the described effects to components which are subjected to a direct bias voltage and thereby high Ar^+ ion bombardment (e.g., focus rings) in the vicinity of the silicon wafer. Components experiencing low ion energy bombardment (eg, Y_2O_3 coatings at the chamber walls) are more likely to show an erosion behavior that is driven by chemical interaction with the reactive fluorine species.

3.2 | Reaction layer formation under varied bias voltages

The second part of the study deals with the chemical interactions and microstructural changes in the near-surface area after the exposure to reactive plasma. Here, the DC self-bias voltage was varied among 50, 150, and 300 V to determine its influence on the erosion behavior. In addition to surface phenomena, the investigation of bias-dependent changes will help to develop a complete understanding of the erosion behavior of yttria in fluorine-based etching plasmas.

At first, physical damage and microstructural changes due to ion bombardment during plasma treatment were investigated by HR-TEM (Figure 6). When increasing the bias voltage from 50 to 300 V, the depth of damage to the crystalline structure became clearly pronounced. Almost no damage was visible at 50 V. Raising the voltage to 150 and 300 V leads to a distorted lattice showing areas having an amorphous appearance up to a depth of around 10 and 15 nm, respectively. Below the damaged zone, no obvious changes in the crystal structure were observed. The HR-TEM images reveal that the chemical reaction at the surface is superposed by the physical damage caused by the Ar ion bombardment. The strong lattice damage visible in samples subjected to 300 V bias voltage could furthermore lead to a suppression of the orientation-dependent erosion mechanisms described in Section 3.1.

Furthermore, STEM and TEM-EDS were used to characterize the influence of bias voltage on the chemical and microstructural development. Figure 7 shows STEM images of the surface layer formed after a plasma exposure of 2 hours under 50 and 300 V. Depending on the bias voltage, a clear difference in the appearance of the affected zone was found. The sample exposed to a bias voltage of 50 V exhibits two layers with a distinguishable appearance, the top layer having a thickness of 14 ± 1 nm, and the bottom layer of 12 ± 2 nm. The related EDS scans reveal a difference in the chemical composition of these layers: the upper layer consists of a fluorine-rich phase probably due to the direct contact with highly reactive species in the plasma, while the layer below shows a more balanced amount of oxygen and fluorine. In comparison to the reaction layer thickness of 8 nm estimated by Kim et al using XPS analysis on samples subjected to bias voltages from 300 to 800 V,[22] the present results of STEM analysis show an increased depth of chemical interaction up to 35 nm. These differences can be induced by lower sputtering rates at voltages between 50 and 300 V allowing increased chemical interaction.

STEM images of the reaction layer formed at bias voltages of 300 V show an increased thickness of the affected zone (44 ± 3 nm). Compared to the affected zone at lower voltages (50-150 V), an additional top layer is visible that exhibits a porous surface, characterized by darker areas and lower intensities in the EDS scan. The porous top layer described in Section 3.1 could be induced by predominant removal of fluorine containing phases from the surface and can lead to a decreased amount of material and, therefore, lower EDS intensities. Additionally, the corresponding EDS scans show a lower fluorine intensity in this porous layer compared to samples subjected to 50 V bias voltage. The amount of fluorine slightly increases in the layer below but does not reach the intensity measured at lower bias voltages. This could be related to the stronger influence of ion sputtering at higher bias voltages, which is coupled with a faster removal of the fluorinated top layer and increased ion damage to the underlying material, as already observed in HR-TEM imaging.

Additionally, the appearance of the microstructure and the pronounced chemical gradient of samples treated at high bias voltage hint at progressive surface erosion through high energy ion bombardment. This leads to the

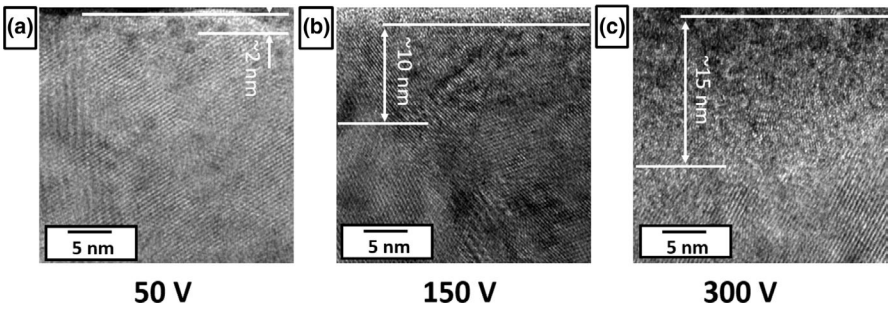

FIGURE 6 HR-TEM images of Y_2O_3 exposed to reactive fluorine plasma, focused on the near-surface area, displaying an ion-damaged top layer, and the unaffected zone below for samples exposed to bias voltages of 50 V (a), 150 V (b), and 300 V (c).

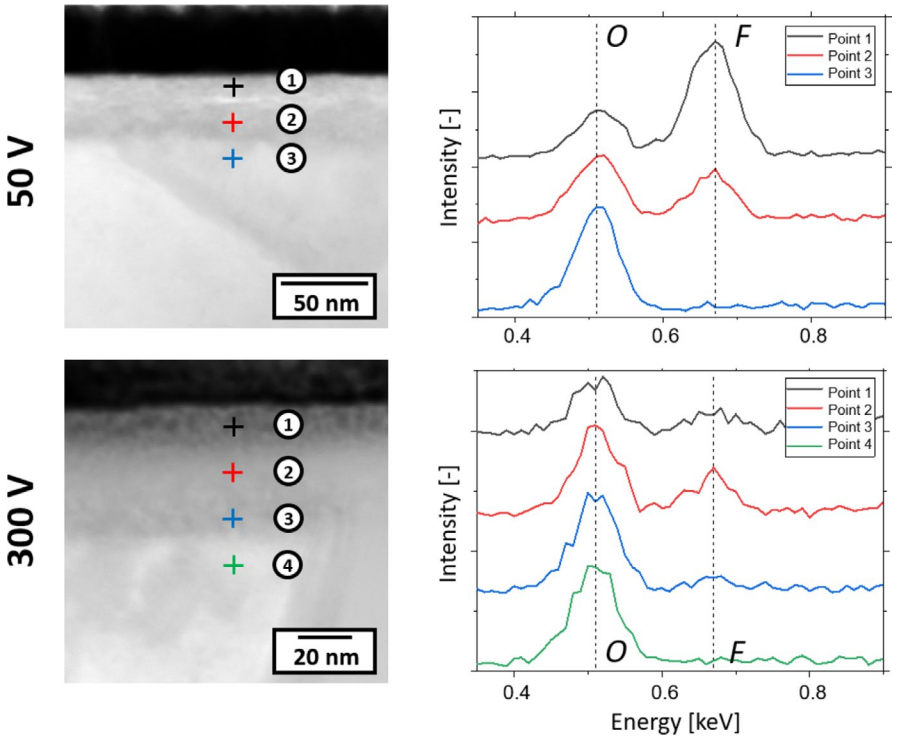

FIGURE 7 (Left) STEM cross-sectional images of the near-surface reaction layer formed after plasma exposure at bias voltages of 50 V (top) and 300 V (bottom). The colored lines highlight the position of TEM-EDS point scans located in surface layers exhibiting microstructural differences. (Right) Corresponding TEM-EDS point scans displaying the intensity peaks of oxygen and fluorine. TEM, transmission electron microscopy [Color figure can be viewed at wileyonlinelibrary.com]

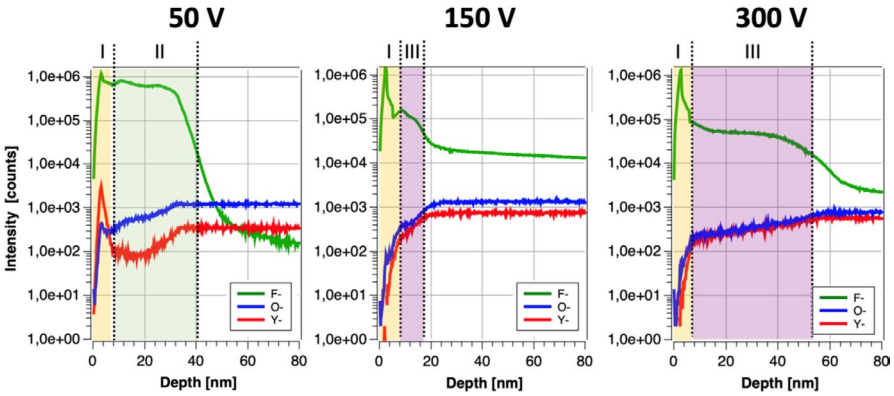

FIGURE 8 Time of flight secondary ion mass spectroscopy depth profiles displaying the intensities of Y, O, and F for samples exposed to bias voltages of 50, 150, and 300 V. Background color highlights the different characteristics of fluorine intensity depending on the applied voltage: (I) high fluorine surface peak, (II) high fluorine intensity layer at low bias voltages, and (III) decreased fluorine intensity layer at high bias voltages. [Color figure can be viewed at wileyonlinelibrary.com]

predominant removal of YF_3 from the surface, generating a top layer with a porous appearance. Sputtering yield studies of Y_2O_3 and the corresponding fluoride YF_3 conducted by Kim et al revealed yield four times higher for the fluoride compound, which could explain the depletion of the fluoride phase in the top layer at the 300 V bias voltage.[23]

The results of TEM-EDS analysis with varying bias voltages permit a sound conclusion on the stages of erosion and material loss during plasma exposure. Continuous surface and near-surface fluorination lead to the formation of YF_3 and YOF compounds which are continuously subjected to Ar^+ ion sputtering. Therefore, it can be concluded that at first the chemical surface reaction is responsible for the depletion of Y_2O_3, but the subsequent material removal process is mainly controlled by the physical sputtering of the surface layer through Ar^+ ions. Although the EDS analysis displays a chemical interaction that occurs to a depth of 35 nm for samples treated with 50 V, this effect does not deteriorate the crystal structure to the same extent as proven by HR-TEM, which is a clear indication of a decoupled erosion mechanism.

For comparison with TEM-EDS results and for gaining an increased understanding of the formation of chemical gradients depending on bias voltage, TOF-SIMS depth profiles were measured, focusing on oxygen, fluorine, and yttrium

content near the surface (Figure 8). The fluorine gradient formed during the plasma treatment depends on the applied bias voltage. Low voltage treatment leads to the formation of a homogeneous fluorine layer (Zone II) of 35 nm in thickness, which slightly decreases in intensity before dropping to a minimum. Under these conditions, the chemical reaction leading to the fluorination of the surface is the dominating mechanism. This observation is in agreement with the results of HR-TEM, where almost no lattice damage is visible, as well as with EDS point analysis, which indicates a comparable gradient. In contrast, the use of intermediate and high bias voltages of 150 and 300 V leads to a reaction layer primarily dominated by physical sputtering (Zone III). In these cases, the distribution of fluorine concentration is separated into two parts: a high-intensity fluorine peak at the surface (I) and a lower-intensity zone, the depth of which depends on the applied voltage (III). The fluorine peak (I) can be related to a characteristic fluorocarbon layer, which is continuously deposited during the exposure to reactive plasmas containing CF_4.[21] The oxygen depth profile exhibits the reverse behavior with respect to the fluorine content, which hints at the substitution of oxygen atoms by fluorine atoms as first described by Miwa et al.[21]

The SIMS results clearly illustrate the strong influence of applied bias voltage on the reaction layer formation. Low bias voltages of 50 V allow the reactive species to form a homogeneous fluorine-enriched top layer, while physical sputtering can be almost neglected. If the bias voltage is increased to 150 V or beyond, significant change in the chemical gradient results.

The high fluorine concentration at surface (I) is caused by the continuous chemical reaction of yttria with the reactive fluorine species in the plasma atmosphere, whereas the gradient below surface (II,III) is controlled by the applied voltage, reaching deeper into the material as the voltage increases. The interaction between chemical surface reaction and physical ion sputtering is responsible for the severity, as well as the depth of damage to the material and therefore has a major impact on the durability during application.

4 | CONCLUSIONS

Polycrystalline yttria is a promising material for components in plasma devices for semiconductor production due to higher resistance against erosion than established silica. Nevertheless, the exact mechanism of interaction between plasma and the yttria grains is still not completely understood. Therefore, polycrystalline yttria samples with a density above 99.9 % were exposed for 2 hours to a reactive CF_4 plasma at varying DC self-bias voltages. Characterization of the surface before and after plasma treatment revealed an erosion mechanism that depends on the grain orientation, resulting in the formation of a plateau-like topography. In EBSD measurements, the topographic height difference could be correlated with the rotation angles Φ and φ_2, showing the maximum height difference in the case of (001) and (011) orientations. This could be caused by an increased "ion transparency" along aligned crystallographic planes leading to lower sputtering yields for certain crystal orientations facing the surface.

Furthermore, changing the bias voltage from 50 to 300 V led to increased physical damage of the top layer as well as the formation of a characteristic fluorine gradient in the near-surface region. TEM and SIMS measurements demonstrated that the physicochemical erosion mechanism strongly depends on the applied bias voltage, which ultimately caused material removal during the plasma exposure and affected the microstructure, the chemical gradient, and the fluorine interaction depth. Due to the very low percentage of porosity inside the microstructure, superposition of fundamental removal mechanisms due to surface defects was prevented to a large extent. Therefore, intrinsic erosion behavior of polycrystalline yttria could be extensively studied, revealing new fundamental insights into the surface plasma interaction.

ACKNOWLEDGMENT

Open access funding enabled and organized by ProjektDEAL.

ORCID

Moritz Kindelmann https://orcid.org/0000-0001-9676-2090
Nino Schön https://orcid.org/0000-0002-1411-7264
Marcin Rasinski https://orcid.org/0000-0001-6277-4421
Rüdiger-A. Eichel https://orcid.org/0000-0002-0013-6325
Florian Hausen https://orcid.org/0000-0001-5712-6761
Martin Bram https://orcid.org/0000-0002-1203-2777
Olivier Guillon https://orcid.org/0000-0003-4831-5725

REFERENCES

1. Nojiri K. Dry etching technology for semiconductors. Cham, Switzerland: Springer International Publishing; 2015.
2. Kim Y-C, Kim C-I. Etching mechanism of Y_2O_3 thin films in high density Cl_2/Ar plasma. J Vac Sci Technol, A. 2001;19(5):2676–9.
3. Iwasawa J, Nishimizu R, Tokita M, Kiyohara M, Uematsu K. Plasma-resistant dense yttrium oxide film prepared by aerosol deposition process. J Am Ceram Soc. 2007;90(8):2327–32.
4. Kim D-M, Oh Y-S, Kim S, Kim H-T, Lim D-S, Lee S-M. The erosion behaviors of Y_2O_3 and YF_3 coatings under fluorocarbon plasma. Thin Solid Films. 2011;519(20):6698–702.
5. Leech PW. Reactive ion etching of quartz and silica-based glasses in CF_4/CHF_3 plasmas. Vacuum. 1999;55(3):191–6.
6. Donnelly VM, Kornblit A. Plasma etching: yesterday, today, and tomorrow. J Vac Sci Technol, A. 2013;31(5):050825.
7. Jung J-H, Hahn B-D, Yoon W-H, Park D-S, Choi J-J, Ryu J, et al. Halogen plasma erosion resistance of rare earth oxide films

deposited on plasma sprayed alumina coating by aerosol deposition. J. Eur. Ceram. Soc. 2012;32(10):2451–7.
8. Ashizawa H, Kiyohara M. Plasma exposure behavior of yttrium oxide film formed by aerosol deposition method. IEEE Trans Semicond Manuf. 2017;30(4):357–61.
9. Cao Y-C, Zhao L, Luo J, Wang K, Zhang B-P, Yokota H, et al. Plasma etching behavior of Y_2O_3 ceramics: comparative study with Al_2O_3. Appl Surf Sci. 2016;366:304–9.
10. Lin T-K, Wang W-K, Huang S-Y, Tasi C-T, Wuu D-S. Comparison of erosion behavior and particle contamination in mass-production CF_4/O_2 plasma chambers using Y_2O_3 and YF_3 protective coatings. Nanomaterials. 2017;7(7):183.
11. Kitamura J, Tang Z, Mizuno H, Sato K, Burgess A. Structural, mechanical and erosion properties of yttrium oxide coatings by axial suspension plasma spraying for electronics applications. J Therm Spray Technol. 2011;20(1):170–85.
12. Zhao D, Wang C, Chen Y, Wang Y. Phase composition, structural, and plasma erosion properties of ceramic coating prepared by suspension plasma spraying. Int J Appl Ceram Technol. 2018;15(6):1388–96.
13. Kim CS, Kim MJ, Cho H, Park T-E, Yun Y-H. Fabrication and plasma resistance of Y_2O_3 ceramics. Ceram Int. 2015;41(10): 12757–62.
14. Ashizawa H, Yoshida K. Effect of the microstructures of yttria ceramics on their plasma corrosion behavior. Ceram Int. 2019;45(17):21162–7
15. Choi K-Y, Oh Y-S, Kim S, Lee S-M. High erosion resistant Y_2O_3–carbon electroconductive composite under the fluorocarbon plasma. Ceram Int. 2013;39(2):1209–14.
16. Kim D-M, Lee S-H, Alexander WB, Kim K-B, Oh Y-S, Lee S-M. X-ray photoelectron spectroscopy study on the interaction of yttrium-aluminum oxide with fluorine-based plasma. J Am Ceram Soc. 2011;94(10):3455–9.
17. Shiba Y, Teramoto A, Goto T, Kishi Y, Shirai Y, Sugawa S. Stable yttrium oxyfluoride used in plasma process chamber. J Vac Sci Technol, A. 2017;35(2):021405.
18. Tsunoura T, Yoshida K, Yano T, Kishi Y. Fabrication, characterization, and fluorine-plasma exposure behavior of dense yttrium oxyfluoride ceramics. Jpn J Appl Phys. 2017;56(6S2):06HC2.
19. Ma T, List T, Donnelly VM. Comparisons of NF_3 plasma-cleaned Y_2O_3, YOF, and YF_3 chamber coatings during silicon etching in Cl_2 plasmas. J Vac Sci Technol, A. 2018;36(3):031305.
20. Kim Y-C, Kim C-I. Etching mechanism of Y_2O_3 thin films in high density Cl_2/Ar plasma. J Vac Sci Technol, A. 2001;19(5): 2676–9.
21. Miwa K, Takada N, Sasaki K. Fluorination mechanisms of Al_2O_3 and Y_2O_3 surfaces irradiated by high-density CF_4/O_2 and SF_6/O_2 plasmas. J Vac Sci Technol, A. 2009;27(4):831–5.
22. Kim D-M, Lee S-H, Alexander WB, Kim K-B, Oh Y-S, Lee S-M. X-ray photoelectron spectroscopy study on the interaction of yttrium-aluminum oxide with fluorine-based plasma. J Am Ceram Soc. 2011;94(10):3455–9.
23. Kim D-M, Jang M-R, Oh Y-S, Kim S, Lee S-M, Lee S-H. Relative sputtering rates of oxides and fluorides of aluminum and yttrium. Surf Coat Technol. 2017;309:694–7.
24. Kim D-M, Kim K-B, Yoon S-Y, Oh Y-S, Kim H-T, Lee S-M. Effects of artificial pores and purity on the erosion behaviors of polycrystalline Al_2O_3 ceramics under fluorine plasma. J Ceram Soc Japan. 2009;117(1368):863–7.
25. Balden M, Bardamid AF, Belyaeva AI, Slatin KA, Davis JW, Haasz AA, et al. Surface roughening and grain orientation dependence of the erosion of polycrystalline stainless steel by hydrogen irradiation. J Nucl Mater. 2004;329-333:1515–9.
26. Voitsenya VS, Balden M, Belyaeva AI, Alimov VK, Tyburska-Püschel B, Galuza AA, et al. Effect of sputtering on self-damaged recrystallized W mirror specimens. J Nucl Mater. 2013;434(1):375–81.
27. Rasinski M, Kreter A, Torikai Y, Linsmeier C. The microstructure of tungsten exposed to D plasma with different impurities. Nucl Mater Energy. 2017;12:302–6.
28. Yoshida H, Morita K, Kim B-N, Hiraga K, Kodo M, Soga K, et al. Densification of nanocrystalline yttria by low temperature spark plasma sintering. J Am Ceram Soc. 2008;91(5):1707–10.
29. Roosendaal HE. Sputtering yields of single crystalline targets. R Behrisch, editor. In Sputtering by particle bombardment I. Berlin, Heidelberg: Springer; 1981. p. 219–56.
30. Onderdelinden D. The influence of channeling on Cu single-crystal sputtering. Appl Phys Lett. 1966;8(8):189–90.
31. Yu LS, Harper JME, Cuomo JJ, Smith DA. Control of thin film orientation by glancing angle ion bombardment during growth. J Vac Sci Technol, A. 1986;4(3):443–7.
32. Dong L, Srolovitz DJ. Mechanism of texture development in ion-beam-assisted deposition. Appl Phys Lett. 1999;75(4):584–6.
33. Dong L, Zepeda-Ruiz LA, Srolovitz DJ. Sputtering and in-plane texture control during the deposition of MgO. J Appl Phys. 2001;89(7):4105–12.

SUPPORTING INFORMATION

Additional supporting information may be found online in the Supporting Information section.

How to cite this article: Kindelmann M, Stamminger M, Schön N, et al. Erosion behavior of Y_2O_3 in fluorine-based etching plasmas: Orientation dependency and reaction layer formation. *J Am Ceram Soc*. 2021;104:1465–1474. https://doi.org/10.1111/jace.17556